Bone Reports 20 (2024) 101744

Contents lists available at ScienceDirect

Bone Reports

journal homepage: www.elsevier.com/locate/bonr

Strontium ranelate retards disc degradation and improves endplate and bone micro-architecture in ovariectomized rats with lumbar fusion induced – Adjacent segment disc degeneration

Qi Sun [a], Fang Liu [b], Jiakang Fang [c], Qiangqiang Lian [c], Yunpeng Hu [c], Xinyu Nan [c], Fa-Ming Tian [b], Guochuan Zhang [d], Dianwen Qi [d], Liu Zhang [e], Jingwen Zhang [f], Yang Luo [g], Zuzhuo Zhang [h], Zhuang Zhou [d,*]

[a] Department of Orthopedic Surgery, The First Hospital of Hebei Medical University, Shijiazhuang, People's Republic of China
[b] Medical Research Center, North China University of Science and Technology, Tangshan, People's Republic of China
[c] Department of Orthopedic Surgery, The Affiliated Hospital of North China University of Science and Technology, Tangshan, People's Republic of China
[d] Department of Musculoskeletal Oncology, The Third Hospital of Hebei Medical University, Shijiazhuang, People's Republic of China
[e] Department of Orthopedic Surgery, Emergency General Hospital, Beijing, People's Republic of China
[f] Department of Neurosurgery, The Second Hospital of Hebei Medical University, Shijiazhuang, China
[g] Department of Orthopedic Surgery, The Third Hospital of Hebei Medical University, Shijiazhuang, People's Republic of China
[h] Department of Radiology, the Third Hospital of Hebei Medical University, Shijiazhuang, People's Republic of China

ARTICLE INFO

Keywords:
Strontium Ranelate
Adjacent segment disc degeneration
Osteoporosis
Rat
Ovariectomy
Lumbar fusion

ABSTRACT

Objectives: Adjacent segment disc degeneration (ASDD) is one of the long-term sequelae of spinal fusion, which is more susceptible with osteoporosis. As an anti-osteoporosis drug, strontium ranelate (SR) has been reported to not only regulate bone metabolism but also cartilage matrix formation. However, it is not yet clear whether SR has a reversal or delaying effect on fusion-induced ASDD in a model of osteoporosis.

Materials and methods: Fifth three-month-old female Sprague-Dawley rats that underwent L4-L5 posterolateral lumbar fusion (PLF) with spinous-process wire fixation 4 weeks after bilateral ovariectomy (OVX) surgery. Animals were administered vehicle (V) or SR (900 mg/kg/d) orally for 12 weeks post-PLF as follows: Sham+V, OVX + V, PLF + V, OVX + PLF + V, and OVX + PLF + SR. Manual palpation and X-ray were used to evaluate the state of lumbar fusion. Adjacent-segment disc was assessed by histological (VG staining and Scoring), histomorphometry (Disc Height, MVD, Calcification rate and Vascular Bud rate), immunohistochemical (Col-II, Aggrecan, MMP-13, ADAMTS-4 and Caspase-3), and mRNA analysis (Col—I, Col-II, Aggrecan, MMP-13 and ADAMTS-4). Adjacent L6 vertebrae microstructures were evaluated by microcomputed tomography.

Results: Manual palpation and radiographs showed clear evidence of the fused segment's immobility. After 12 weeks of PLF surgery, a fusion-induced ASDD model was established. Low bone mass caused by ovariectomy can significantly exacerbate ASDD progression. SR exerted a protective effect on adjacent segment intervertebral disc with the underlying mechanism possibly being associated with preserving bone mass to prevent spinal instability, maintaining the functional integrity of endplate vascular microstructure, and regulating matrix metabolism in the nucleus pulposus and annulus fibrosus.

Discussion: Anti-osteoporosis medication SR treatments not only maintain bone mass and prevent fractures, but early intervention could also potentially delay degenerative conditions linked to osteoporosis. Taken together, our results suggested that SR might be a promising approach for the intervention of fusion-induced ASDD with osteoporosis.

* Corresponding author at: Department of Musculoskeletal Oncology, The Third Hospital of Hebei Medical University, 361 Zhongshan E Rd, Shijiazhuang, Hebei 063000, China.
E-mail address: 38500453@hebmu.edu.cn (Z. Zhou).

https://doi.org/10.1016/j.bonr.2024.101744
Received 22 September 2023; Received in revised form 2 February 2024; Accepted 12 February 2024
Available online 15 February 2024

1. Introduction

Osteoporosis is a widespread systemic osteometabolic disorder, which can affect people of all ethnic backgrounds and especially in postmenopausal women, is characterized by low bone mass and microarchitectural deterioration of bone tissue, leading to enhanced bone fragility and increased fracture risk (Compston et al., 2019). Hip and clinical vertebral fractures are the most devastating consequences of osteoporosis and are associated with increased morbidity and mortality (Ensrud and Crandall, 2017). In addition to causing pathological fractures, osteoporosis can also aggravates the progression of other diseases, such as osteoarthritis (Calvo et al., 2007), disc degeneration (Lou et al., 2017) and femur head osteonecrosis (Gangji et al., 2018) et al.

Adjacent segment disc degeneration (ASDD) is one of the long-term sequelae of spinal fusion , which currently considered the "gold standard" among surgical procedures used to address various lumbar pathologies, including lumbar stenosis, instability and discogenic pain (Zhou et al., 2016; Ishihara et al., 2001). Altered segment biomechanics and kinematic functions at neighboring levels are widely assumed to be causative factors for ASDD, however, the etiology of ASDD is still not fully clarified and some are conflicting (Kamali et al., 2021). In epidemiology, the prevalence of osteoporosis and adjacent segment disc degeneration shares similar characteristics with aging, especially in postmenopausal women. Estrogen's profound impact on bone matrix turnover carries crucial implications, encompassing the preservation of tissue structure appearance and the maintenance of strength and stiffness in various structures (Calleja-Agius and Brincat, 2009). In addition to changing mechanical properties , estrogen deficiency exacerbated IDD induced by spinal instability, endplate degeneration, and also affect metabolic of disc (Liu et al., 2019; Luo et al., 2013). There is evidence that osteoporosis leads to the deterioration of biomechanical characteristics in the adjacent segment disc in clinical (Zhou et al., 2016; Li et al., 2019; Etebar and Cahill, 1999). In our previous animal study (Zhou et al., 2016; Zhou et al., 2015; Liu et al., 2015), we also confirmed that ovariectomy can accelerate the progression of the ASDD in rat. Furthermore, re-operation is the ultimate choice for ASDD (Burch et al., 2020), and the situation in patients with osteoporosis may be progress faster and more serious than ASDD alone.

Strontium ranelate (SR) is an anti-osteoporotic drug with a unique dual effect on bone formation and resorption. It regulates bone cell differentiation, stimulates osteoblast growth, and suppresses osteoclast formation. SR also reduces matrix metalloproteinase (MMP) production and modulates the osteoprotegerin-RANKL pathway, inhibiting osteoclastic activity (Reginster et al., 2005). In addition to has proven effective in patients with osteoporosis, SR has reportedly can regulate cartilage metabolism, indicating SR may act as a DMOAD in the treatment of OA (Tat et al., 2011). MMP-1, MMP-13 gene expression in OA cartilage can be inhibited by SR, as well as IL-1β and MMP-3 in OA synovium (Pelletier et al., 2013). SR also showed Increases cartilage matrix formation, which stimulate the synthesis of type II collagen and proteoglycan (Henrotin et al., 2001). In knee OA patients, treatment with SRan 2 g/day was found to have beneficial effects on structural changes by significantly reducing cartilage volume loss in the plateau and bone marrow lesions progression in the medial compartment (Pelletier et al., 2015). In view of the higher risk of postoperative complications and economic burden of reoperation in osteoporotic patients with ASDD, benefits should be reconsidered toward potential DMOAD effect verse cardiac events issued by European Medicines Agency (EMA) in specific situation (accessed 4 November, 2013), especially in patients without cardiac risks.

Considering the existing evidence of SR action on both bone and cartilage metabolism and rare study involving the action of this drug on osteoporotic ASDD, the objective of this study was to investigate whether SR, a dual action anti-osteoporotic agent with potential DMOAD effect on cartilage, could not only prevent bone loss, but also retard osteoporotic ASDD progression in ovariectomized rat, providing evidence for clinical decision.

Table 1
Radiographic Scoring System by O'Loughlin et al.

Descriptions	Score
No Bone	0
Poor new bone formation and definite pseudo arthrosis	1
Moderate new bone formation and definite pseudoarthrosis	2
Good new bone formation and possible pseudoarthrosis	3
Good new bone formation and probable fusion	4
Definite fusion	5

2. Materials and methods

2.1. Experimental animals, models and reagents

All procedures regarding housing, breeding, and collection of animal tissues were performed as per approved protocols by Institutional Animal Care and Use Committee (IACUC). All rats were allowed free access to water and a maintenance diet. All cages contained wood shavings, bedding and a cardboard tube for environment enrichment. All rats were kept under a 12 h light/dark cycle at a constant temperature of 25 °C.

Fifty-three-month-old female healthy Sprague-Dawley (SD) rats were randomly divided into five groups as follows: Sham+V, OVX + V, PLF + V, OVX + PLF + V, OVX + PLF + SR. Four weeks after bilateral ovariectomy (OVX) surgery, rats underwent modified posterolateral lumbar fusion (PLF) at L4–5. SR or vehicle were given by oral gavage at a dosage of 900 mg/kg/d around 9:00 AM for 12 weeks. Control groups were set up accordingly, normal saline was given to OVX + PLF + V group as a placebo control and treatment lasted for 12 weeks. The dose of normal saline and SR were adjusted weekly depending on body weight. All animals were euthanized at 12 weeks by intraperitoneal overdose injection of Ketamine and Xylazine, whole lumbar spines were harvested.

2.2. Surgical procedures for OVX model and PLF model

An electric razor was used to remove hair from the surgical site, followed by disinfected with povidone-iodine solution and 75 % ethanol. Rats were anesthetized via an intraperitoneal injection with a combination of Ketamine and Xylazine. Ovariectomy was performed via bilateral incisions in the skin and small bilateral sections through the muscle layer at the angle between the last rib and vertebral column. The skin was incised together with the dorsal muscles and the peritoneal cavity was accessed. The ovary was identified, surrounded by a variable amount of fat. After vascular ligation, the connection between the fallopian tube and the uterine horn was cut and the ovary removed. PLF were performed 4 weeks after surgery, briefly, rats were positioned prone and prepared in the standard surgical fashion. The spine was approaches through a single midline skin incision between L3 and L6 levels, and two paramedian fascial incisions (Wiltse approach) were then made to expose the posterior/facet joints between L3 and L6. The transverse processes were decorticated with a blade until a cancellous bone was observed. Approximately 0.2 g of cortico-cancellous bone was harvested from the iliac crest, cut into small pieces, and then grafted at the L4-L5 interarticular spaces. Steel wire was used to bind the spinous processes of L4 and L5 to fix L4–5 segment, as described by Dimar and colleagues (Dimar 2nd et al., 1996). Wound were closed, and prophylactic antibiotics (Penicillin-G; 40,000 U) were given soon after surgery for 3 days.

2.3. Fusion evaluation by radiograph and manual palpation

Immediate radiographic investigation (Anteroposterior Position, DR7500 System, Kodak, USA) took place for each subject right after the euthanizing process. Imaging was graded using the criterion described

Table 2
Lumbar Disc Degeneration Assessment Scoring System By Wang et al.

Score	Nucleus Pulposus	Annulus Fibrosus	Osteophyte
0	Bulging gel with abundant notochordal cells	Compact fibrous lamellas	Absence
1	Notochordal cells loss; chondrocyte-like cells emergence	Proliferation of fibrocartilaginous tissue and loss of nuclear–annular border	Appearance
2	Focal mucoid degeneration; clefts	Fissures in annulus fibrosis	Overgrowth
3	Diffuse mucoid degeneration and clefts throughout nucleus		

by O'Loughlin *et al* (O'Loughlin et al., *2009*) (Table 1).

After the radiographic investigation, lumbar spines of subjects were excised, and soft tissues removed. Fusion assessment with manual palpation depended on a previously used method by Abe et al (Abe et al., 2007). Flexion, extension, and lateral flexion were tested by three observers in a blinded manner. Lack of motion was defined as successful fusion. Manual Palpation is the gold standard method for detecting mobility and stability of the fusion site (DePalma and Rothman, 1968).

2.4. Micro-CT measurement

Right after fusion assessment, L6 segment were scanned using a Skyscan 1176 micro-CT with 18 um per-voxel resolution (80 Kv, 313 uA). The measurement was similar as previous described. The 3D imaging was developed using CTan software (V1.14), an inner cylinder of 1.5 mm in diameter and 3 mm in length set as the volume of interest. The bone mineral density (BMD), percent bone volume/total volume (BV/TV), trabecular thickness (Tb.Th), trabecular number (Th. N), and trabecular separation (Tb, Sp) were measured.

2.5. Histological assessment, scoring and histomorphometry observation

The L5–6 segment (Lower adjacent segment of fusion) were fixed with 10 % neutral buffered formalin for 48 h and decalcified with EDTA-2Na for three month, embedded in paraffin, deparaffinized in xylene, and rehydrated through a series of ethanol washes. The paraffin blocks were sagittal sectioned at 5 μm thickness with cationic slides and stained with Van Gieson (VG), then captured under microscopic system (BX53, Olympus, Tokyo, Japan) for semi-quantitative microscopic scoring described by Wang et al (Wang et al., 2004) (Table 2). The paraffin blocks were sagittal sectioned at 5 μm thickness with cationic slides and stained with Van Gieson (VG), then captured under microscopic system (BX53, Olympus, Tokyo, Japan) for semi-quantitative microscopic scoring described by Wang et al (Wang et al., 2004) (Table 2). Three observers participated in histological score characterization.

For histomorphometry assessment, the disc height, Microvessel Density(MVD), the ratio of calcification area and ratio of vascular area were based on VG images. Three measurements from three parts of disc, left, center and right side, were averaged to determine the height of disc (Allon et al., 2010). The ratio of calcification area and vascular area were also measured using cellSens Dimension VX Image Processing software (Olympus, Tokyo, Japan) by contouring the calcification area and the vascular area then compared to the total endplate area.

2.6. Immunohistochemical assessment

For further investigation, aggrecan (AGG) (1:500, GTX54920, GeneTex, USA), collagen-II (Col-II) (1:100, II-II6B3, Linsenmayer, T.F.), Aggrecan, a disintegrin and metalloproteinase with thrombospondin motifs 4 (ADAMTS-4) (1:200, ab185722, Abcam, USA), Caspase-3 (1:100, GTX110543, GeneTex, USA) and metalloproteinase-13 (MMP-13) (1:200 dilution, GTX55707, GeneTex, USA) were detected using immunohistochemistry. Briefly, 5 μm thick sections were deparaffinized and rehydrated. Next, sections underwent antigen retrieval and inactivation of endogenous peroxidases prior to incubation with primary antibodies overnight at 4 °C. Sections were washed and incubated with a biotinylated secondary antibody and a streptavidin biotin complex-peroxidase solution. Diaminobenzidine (DAB) chromogen was applied and counterstained with hematoxylin for antibody detection.

Imagines was captured by microscope system (BX53, Olympus, Tokyo, Japan). The integrated optical density (IOD) was semi-quantitatively measured using Imaging Pro Plus 6.0 software (Media Cybernerics, Rockville, MD, USA). By quantifying cumulative optical density (IOD) and area for each image, we calculate mean density as mean density = IOD/area. This value indicates the target parameters' concentration per unit area. The specimen's positivity rate is determined by averaging mean density from 3 random regions (High-magnification images - 40× objective lens) per sample.

2.7. Quantitative real-time PCR for adjacent segment disc

Whole RNA was extracted from L3–4 segment disc (Upper adjacent segment of fusion) by TRIzol (Invitrogen, Carlsbad, USA). The concentration and quality of RNA were assessed using Quawell Q5000 spectrophotmeter (Quawell, San Jose, USA) and Gene Amp 7700 Sequence Detection System (Applied Biosystems, Foster City, CA) was used to carry out reverse transcription reaction on RNA in accordance with protocols of manufacturer. RT-PCR was performed on QuantStudio5 (ThermoFisher, Waltham, USA). Custom-designed, validated primers for Col1α1, Col2α1, Aggrecan, MMP-13 and ADAMTS-4 (Table 3). The change in expression of mRNA was assessed by ΔΔCt-Method using GAPDH as housekeeping gene.

2.8. Statistical analysis

Data were expressed as the mean ± Standard Deviation (SD) and analyzed with SPSS 18.0 software. The significant differences were assessed by one-way analysis of variance (ANOVA) and Fisher least significant difference method. The histological and radiological results were analyzed using Kruskal-Wallis test. $P < 0.05$ was considered statistically significant.

Table 3
The Primers Sequences Used for RT-PCR.

Gene	Accession No.	Forward primer (5′-3′)	Reverse primers (5′-3′)
GAPDH	NM_017008.4	GGGGAGCCAAAAGGGTCATCATCT	GAGGGGCCATCCACAGTCTTCT
Col2α1	NM_053304.1	GGGAATGTCCTCTGCGATGAC	GAAGGGGATCTCGGGGTTG
Col1α1	NM_012929.1	GACTGTCCCAACCCCCAAAA	TGGGTCCCTCGACTCCTATG
Aggrecan	NM_022190.1	GAAGTGGCGTCCAAACCAAC	AGCTGGTAATTGCAGGGGAC
MMP13	NM_133530.1	TGCTGCATACGAGCATCCAT	TTCCCCGTGTCCTCAAAGTG
ADAMTS-4	NM_023959.1	CGTTCCGCTCCTGTAACACT	TTGAAGAGGTCGGTTCGGTG

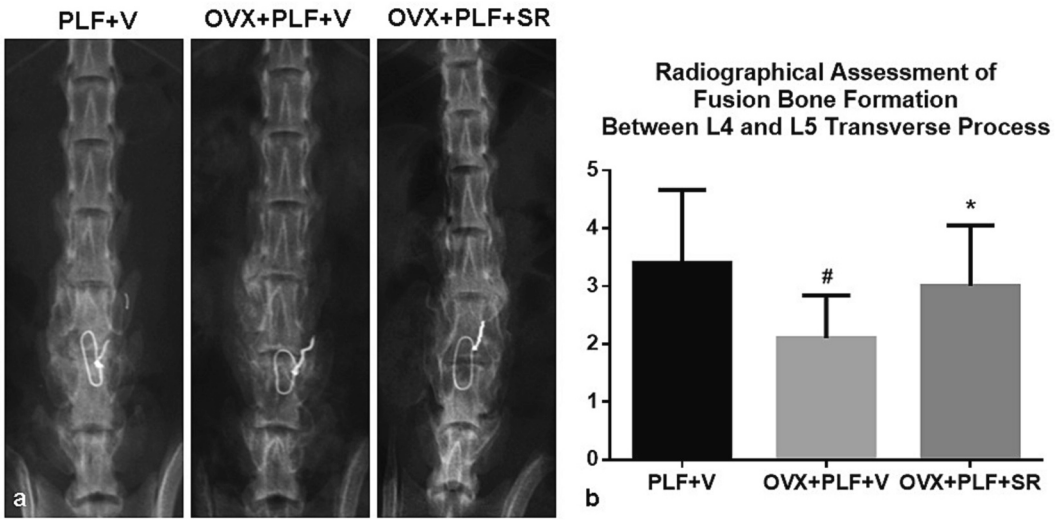

Fig. 1. Radiologic features of L4–5 fusion assessment (a), and radiographic score analysis (b) of new bone formation between transverse processes. The imaging were captured at 12 weeks after PLF surgery, which using an intertransverse process fusion with an autologous iliac bone graft and spinous-process wire fixation. Avoided direct OVX + PLF + SR vs. Sham+V due to complex three variables. OVX + PLF + V group showed lowest score, whereas, SR administration can increase the radiographical score. Note: $^{\#}P < 0.05$ vs. PLF + V group; $^{*}P < 0.05$ vs. OVX + PLF + V group.

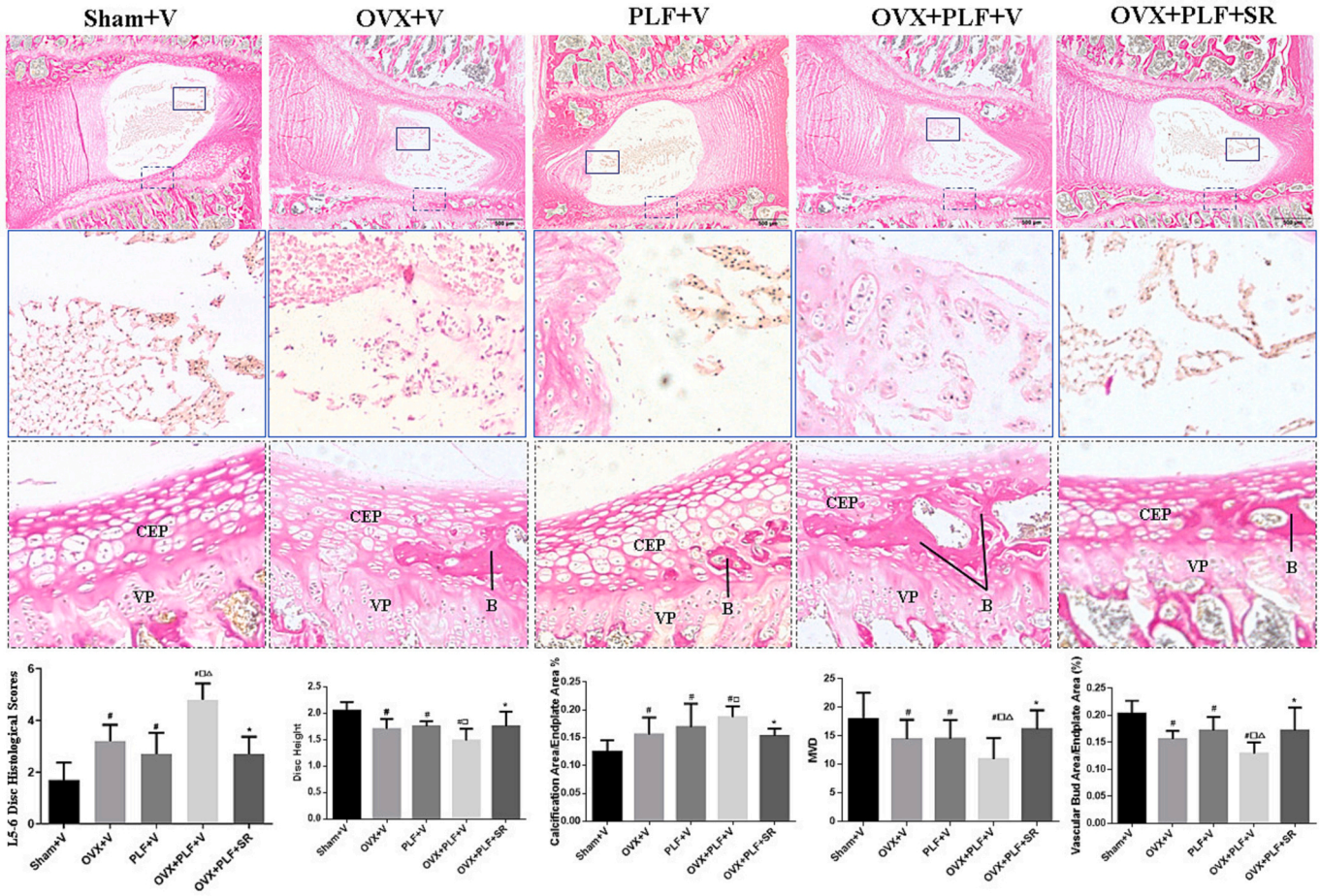

Fig. 2. Histological manifestation, histological score and histomorphometric parameters analysis (disc height, endplate thickness, MVD, the ratio of calcified area and vascular area) of adjacent segment disc (L5–6) at 12 weeks after PLF surgery. Avoided direct OVX + PLF + SR vs. Sham+V due to complex three variables. Note: $^{\#}P < 0.05$ vs. Sham+V group; $^{\square}P < 0.05$ vs. OVX + V group; $^{\triangle}P < 0.05$ vs. PLF + V group; $^{*}P < 0.05$ vs. OVX + PLF + V group. VP, vertebral physis; CEP, cartilage endplate; B, bony tissues.

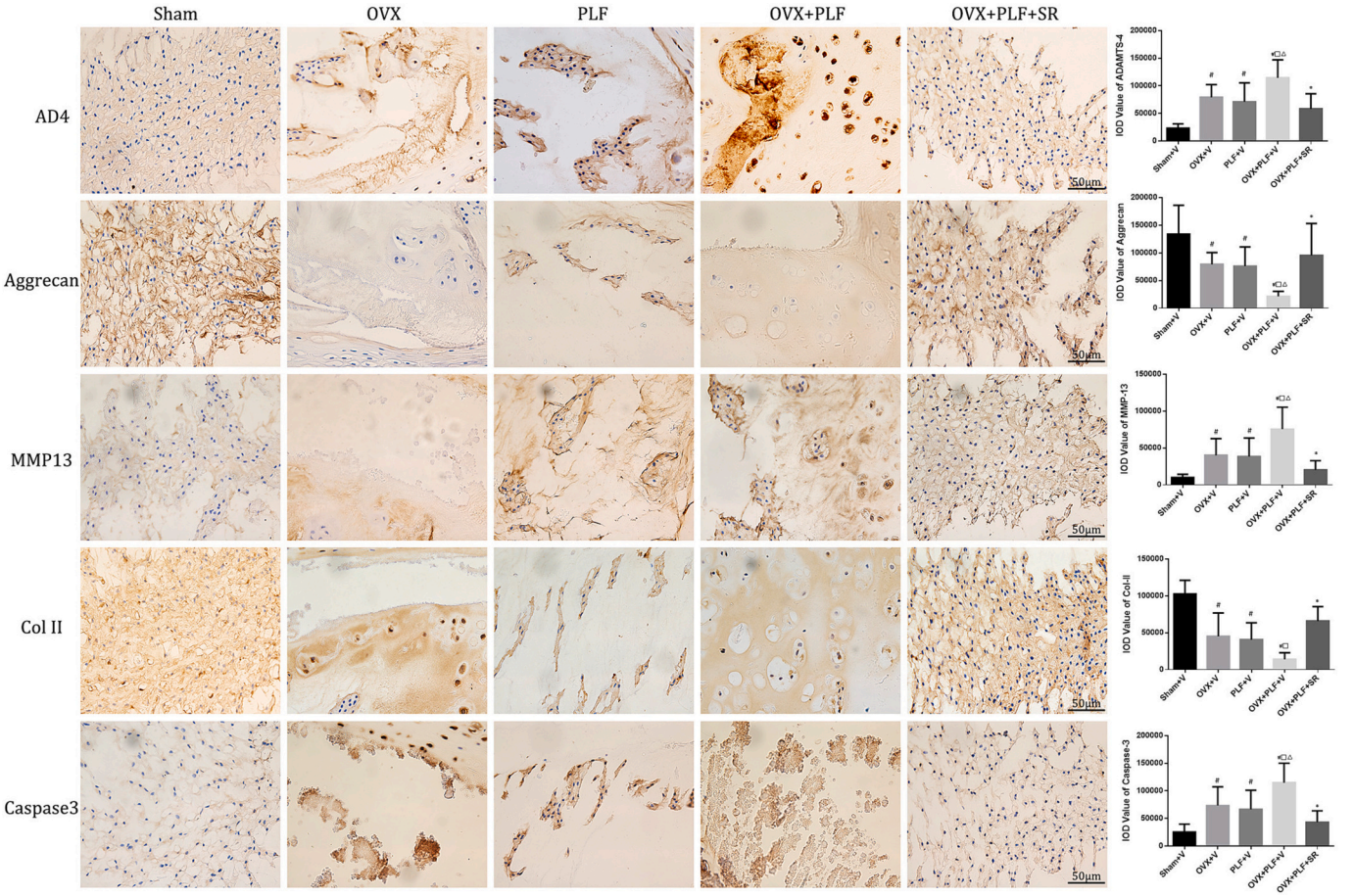

Fig. 3. Imunohistochemical manifestation and immunohistochemistry IOD value (Col-II, Aggrecan, MMP-13, ADAMTS-4 and Caspase-3) in the nucleus pulposus (40×). Avoided direct OVX + PLF + SR vs. Sham+V due to complex three variables. Note: $^{\#}P < 0.05$ vs. Sham+V group; $^{\square}P < 0.05$ vs. OVX + V group; $^{\triangle}P < 0.05$ vs. PLF + V group; $^{*}P < 0.05$ vs. OVX + PLF + V group.

3. Results

3.1. Radiographical and manual palpation evaluation

The newly formed callus was found between transverse process in all PLF samples examined. The radiological score showed higher X-ray score in OVX + PLF + V group, compared with PLF + V group (Fig. 1b), indicating ovariectomy and SR administration are the contributing factors that lead to different healing status. A lower radiographic score is also observed in OVX + PLF + SR group when compared with OVX + PLF + V group (Fig. 1b).

Although the X-ray score vary, we found there were no detectable movement at the fusion site. Wire fixation of spinous process as modified surgical method described by Dimar and colleagues, is an important factor in improving surgical results.

3.2. Histological and histomorphometric analysis

In the Sham+V group, a considerable number of regular cells were discovered enclosed by an extracellular matrix within the nucleus pulposus. The collagen bundles within the lamellae displayed a consistent and orderly parallel alignment. Moreover, the outer annulus fibrosus displayed well-ordered rows. The endplate was rich in hyaline cartilage and contained chondrocytes. In contrast, the OVX + V and OVX + PLF + V groups displayed clusters of atypical cells, often accompanied by enlarged cellular morphology and abnormal staining, resulting in a pronounced decrease in NP cells. Additionally, the surrounding matrix exhibited indications of mucinous degeneration. Various degrees of derangement were observed in the annulus fibrosus. The endplate appeared to have large areas with varying degrees of calcification and contained numerous vascular buds. These degenerative changes were most pronounced in the OVX + PLF + V group, whereas the OVX + PLF + SR group exhibited less severe pathological changes. (Fig. 2).

Fig. 2 also shows that ASDD histologic score in the OVX + PLF + V group was significantly higher compared to that in the control group (Sham+V, OVX + V and PLF + V groups) ($P < 0.05$). However, the histologic score in the OVX + PLF + SR group is significantly lower than that of the OVX + PLF + V group after 12 weeks of SR administration ($P < 0.05$).

The OVX + V, PLF + V, and OVX + PLF + V groups exhibited significantly lower values for disc height, microvessel density (MVD), and vascular bud area/endplate area and higher value for calcification area/endplate area compared to the Sham+V group ($P < 0.05$). In the OVX + PLF + SR group, however, there was a remarkable higher in disc height, MVD, calcification area/endplate area, and vascular bud area/endplate area when compared to the OVX + PLF + V group ($P < 0.05$).

3.3. Immunohistochemical analysis

To investigate the extracellular matrix (ECM) remodeling of adjacent segment disc (ASD), the immunohistochemical staining of Col-II, Aggrecan, ADAMTS-4, MMP-13, and Caspase-3 were conducted.

As an osteoporotic ASDD model group, OVX + PLF + V group showed that the IOD values of Col-II, and Aggrecan were significantly decreased and significantly increased in MMP-13, ADAMTS-4 and Caspase-3 when compared to Sham+V group, OVX + V group and PLF

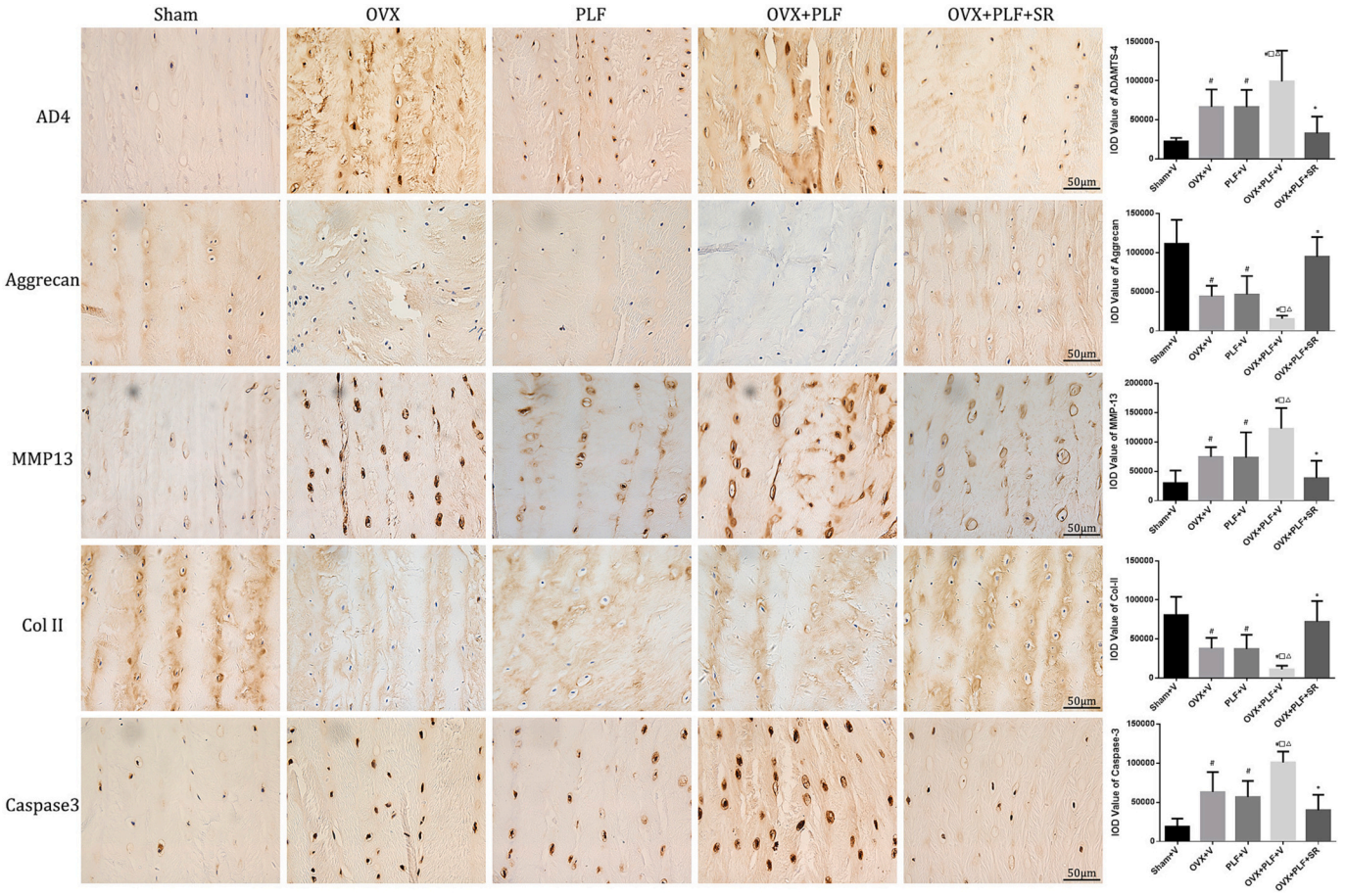

Fig. 4. Imunohistochemical manifestation and immunohistochemistry IOD value (Col-II, Aggrecan, MMP-13, ADAMTS-4 and Caspase-3) in the annulus fibrous (40×). Avoided direct OVX + PLF + SR vs. Sham+V due to complex three variables. Note: $^{\#}P < 0.05$ vs. Sham+V group; $^{\square}P < 0.05$ vs. OVX + V group; $^{\triangle}P < 0.05$ vs. PLF + V group; $^{*}P < 0.05$ vs. OVX + PLF + V group.

+ V group in the NP and AF. However, the IOD value of OVX + PLF + SR group is significantly higher in Col-II, and Aggrecan and significantly lower in MMP-13, ADAMTS-4 and Caspase-3 than OVX++PLF + V group. (Figs. 3 and 4).

3.4. Quantitative real-time PCR analysis

To further elaborate the ECM remodeling, we examined the expression levels of Aggrecan, Col—II, Col-I, ADAMTS-4, and MMP-13 at the NP and AF to confirm whether the changes within ECM are consistent. Real-time RT-PCR detected that both Aggrecan and Col-II were expressed lower, and Col—I, ADAMTS-4, and MMP-13 were expressed higher in OVX + PLF + V group compared to Control group (Sham+V, OVX + V and OVX + PLF + V groups). In the SR group, however, Aggrecan and Col-II were expressed higher, and Caspase-3, ADAMTS-4, and MMP-13 were expressed lower compared with that in OVX + PLF + V group. (Fig. 5).

3.5. Micro-CT analysis

The micro-CT scans demonstrated marked distinctions in the bone microstructure among the five groups. The 3D reconstructed image shows relatively loose bone trabeculae in OVX + V group and OVX + PLF + V group when compared to Sham+V group and PLF + V group, respectively. However, bone trabecular was close-packed in OVX + PLF + SR group when compared to OVX + PLF + V group. (Fig. 6).

Quantitative analyses showed BMD, BV/TV, Tb.Th, and Tb.N were significantly decreased but Tb. Sp was significantly increased in the OVX + V group and OVX + PLF + V group when compared to Sham+V group and PLF + V group, respectively. With the benefit of SR, BMD, BV/TV, Tb.Th, and Tb.N were significantly improved but Tb. Sp was significantly decreased compared to OVX + PLF + V group, suggesting a significant improvement of vertebra microstructure.

4. Discussion

Osteoporosis, in addition to being able to cause pathological fractures, can also exacerbate and accelerate various pathological processes, such as osteoarthritis, intervertebral disc degeneration, etc (Hart et al., 2002; Zhang et al., 2000; Wáng, 2018; Xiao et al., 2018). Confirmed by our current and previous experiments (Zhou et al., 2016), we have observed that OVX exacerbates ASDD following spinal fusion in rats. SR , however, as an anti-osteoporotic medication, not only mitigates estrogen-induced bone loss, but also retards adjacent disc segments degeneration after spinal fusion.

Osteoporotic bone loss impacts both cortical and trabecular (spongy) bone structures (Chen et al., 2013). Cortical thickness decreases, while the quantity and dimensions of trabeculae diminish, leading to higher porosity. Trabecular bone loss exceeds cortical bone loss due to its greater porosity and bone turnover. This weakening of both types of bone contributes to compromised skeletal integrity and changes in spine biomechanics (Zebaze et al., 2019). This change is also considered to involve natural progression of degenerative lumbar spine disease, thereby accelerating intervertebral disc degeneration, intervertebral space stenosis, and vertebral body instability (Wáng, 2018; Tomé-Bermejo et al., 2017; McKiernan, 2009). Moreover, administration of SR

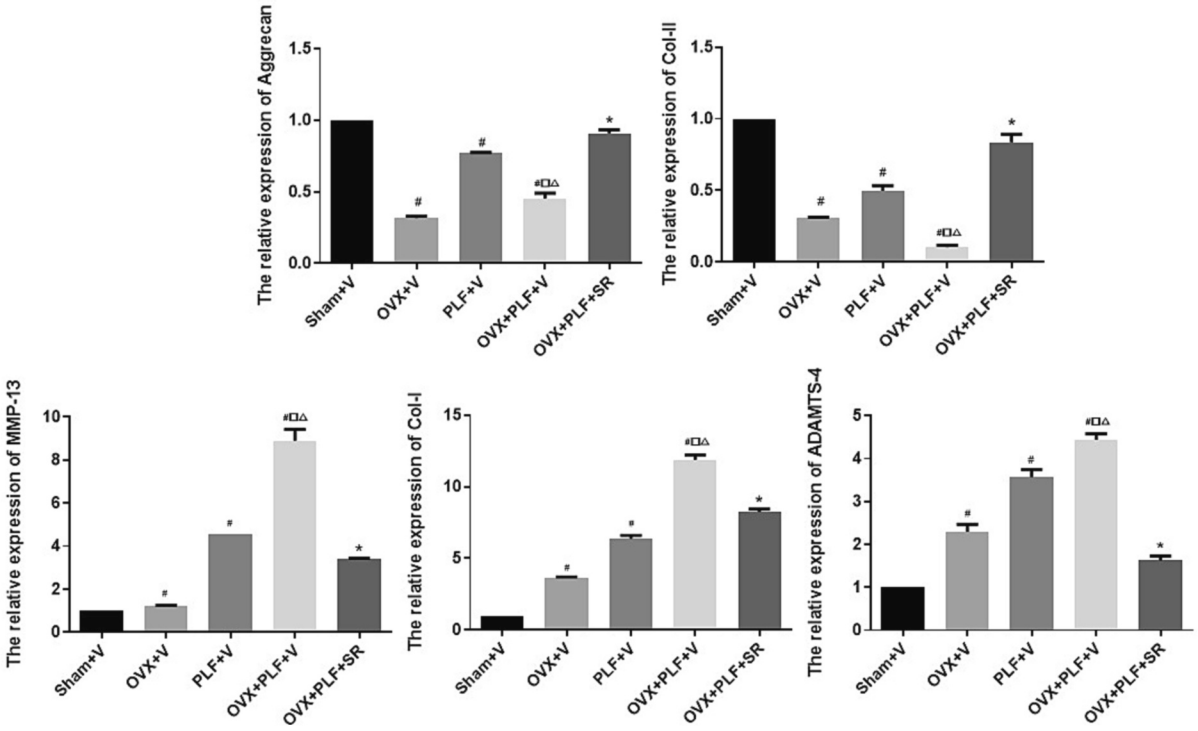

Fig. 5. Relative expression of Col1α1, Col2α1, Aggrecan, MMP-13 and ADAMTS-4 determined by qRT-PCR. Avoided direct OVX + PLF + SR vs. Sham+V due to complex three variables. Note: $^{\#}P < 0.05$ vs. Sham+V group; $^{\square}P < 0.05$ vs. OVX + V group; $^{\triangle}P < 0.05$ vs. PLF + V group; $^{*}P < 0.05$ vs. OVX + PLF + V group.

reportedly exhibited a noteworthy reduction of 31 % in overall clinical fractures related to osteoporosis (including vertebral fractures), and a significant decrease of 40 % specifically in morphometric vertebral fractures (Kanis et al., 2011). This confirms its potential as a successful approach to addressing osteoporotic fractures. In our experiment, it was found that SR can significantly increase bone mass in osteoporotic rats, which plays a crucial role in stabilizing the vertebral bodies and spine. Additionally, activity was not detected at the fusion site through manual testing, indicating that all models achieved the desired surgical outcome.

Spinal fusion is considered the gold standard treatment for multiple lumbar spine issues, producing good clinical results (Pradeep and Pal, 2023). However, postoperative biomechanical changes caused by fusion-related conditions may reduce the initial positive outcomes due to adjacent segment degeneration (Ebrahimkhani et al., 2021). As two diseases with similar onset ages, the reduction of bone mineral density (BMD) caused by osteoporosis may be more likely to develop or exacerbate ASDD progression by adversely changing the loading pattern and intradiscal pressure (Li et al., 2019; Yuan et al., 2022). Jingchi Li *et al (*Li et al., *2019)* reported that osteoporosis leads to the deterioration of biomechanical characteristics in the adjacent segment disc after spine surgery. And Chenchen Zhang *et al (*Zhang et al., *2021)* reported that osteoporosis may mitigate the adverse influence of ALIF on adjacent segments. O Bruyere *et al (*Bruyere et al., *2008)* demonstrated that SR could reduce the progression of the radiographic features of spinal OA and back pain in women with osteoporosis and prevalent spinal OA. In our experiment, we also found that ovariectomy can worsen the progression of adjacent segment degeneration. SR can effectively preserved BMD and structural parameters in the adjacent vertebrae of ovariectomized rats, indicating that the potential protective effect of SR on ASDD may be attributed to the observed optimization of trabecular bone structure in our study. Thus, SR shows promise as a potential effective medication for degenerative diseases specifically related to osteoporosis.

As an avascular structure, the intervertebral disc relies on nutrient diffusion from endplate (Grangeat and Erario, 2023). Calcifications of vertebral endplates with disease have suggested insufficient nutrition as a mechanism for intervertebral disc degeneration (Benneker et al., 2004). It has been suggested that EP calcification is involved in disc degeneration by acting as a barrier to nutrient transport and decreasing nutrient availability to the disc (Gruber et al., 2007). Blood vessels enter through vertebral pores in the cortical shell, forming an arterial network that ends near the cartilaginous endplate. Reduced nutrient supply leads to lower oxygen and higher lactate levels, affecting pH, which impacts cell function and the synthesis of the extracellular matrix of NP and AF (Fields et al., 2018; Velnar and Gradisnik, 2023). In addition, finite-element stress analysis and animal model revealed that spinal instability causes vertebral microarchitecture change and initiate vertebral endplate damage and cause intervertebral disc degeneration (Liu et al., 2020; Mizrahi et al., 1993). Osteoporosis-induced low bone mass and osteochondral remodeling of the cartilaginous endplate contributing to the angiogenesis and an increase in porosity of the bone-cartilage surface, and also affected the matrix metabolism which consequently had detrimental effects on the intervertebral disc (Xiao et al., 2018). Through morphological parameter analysis of VG staining results, our experiment found a significant reduction in microvessel quantity and density in the PLF + V group compared with Sham+V group. The exacerbation of this change in the OVX + PLF + V group indicates that lower BMD can worsen degeneration by decreasing microvessels in the endplate. However, SR effectively preserved microvessels quantity and area in the endplate, suggesting that SR may be involved in preserving the structural integrity and function of adjacent structures by maintaining the quantity and area of microvessels in the endplate and reduce the calcification area of the endplate, which could potentially delaying the disc from degeneration by preserving normal endplate's functionality.

The intervertebral disc is a fibrous cartilage tissue that contains the annulus fibrosus and nucleus pulposus. The NP is a centrally located highly hydrated gel-like tissue surrounded by the AF, comprised of layer-by-layer collagen fiber lamellas. Increased mechanical stress on adjacent segment intervertebral discs and abnormal mechanical stress in

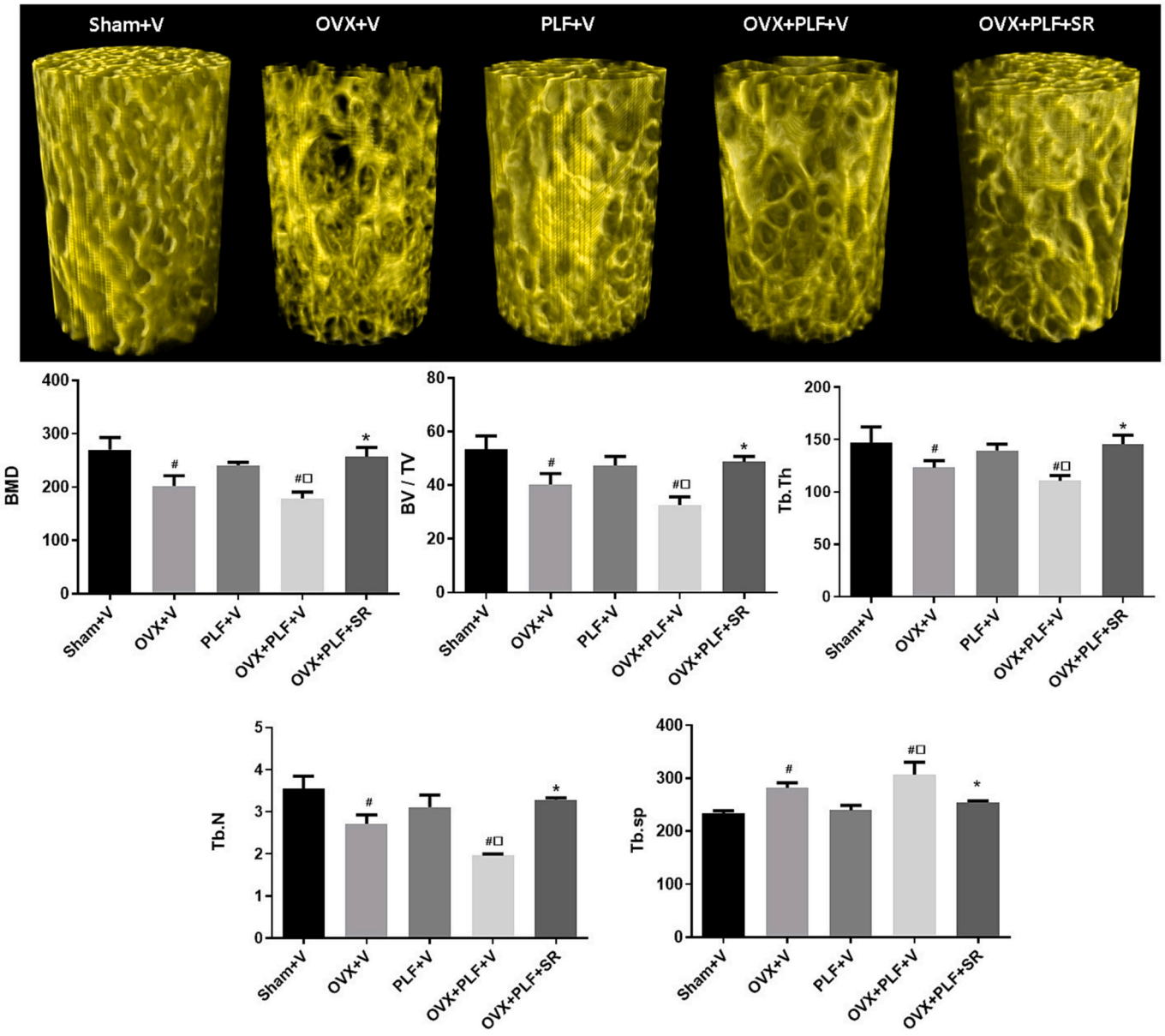

Fig. 6. The bar graphs (mean + SD) show bone morphometric parameters (BMD, BV/TV, Tb.Th, Tb.N and Tb. Sp) and Micro-CT rendered 3-D images morphology illustration of L6 trabecular bone concerning the density of trabecular bone. Avoided direct OVX + PLF + SR vs. Sham+V due to complex three variables. Note: $^{\#}P < 0.05$ vs. Sham+V group; $^{\square}P < 0.05$ vs. OVX + V group; $^{\triangle}P < 0.05$ vs. PLF + V group; $^{*}P < 0.05$ vs. OVX + PLF + V group.

osteoporotic conditions can directly impact intervertebral disc metabolism (Dou et al., 2021). Alternatively, they can lead to intervertebral disc degeneration by regulating the quantity and area of microvessels within the endplate, thereby reducing the nutritional supply to the disc (Nachemson et al., 1970). We also found that ovariectomy significantly enhances the degree of ASDD induced by spinal fusion, leading to increased expression of MMP-13/ADAMTS-4 and reduced expression of type II collagen and Aggrecan (Zhou et al., 2016). Moreover, SR exhibited a discernible retarding effect on the loss of crucial matrix constituents and displayed inhibitory properties against the generation of degradative enzymes. Furthermore, some studies showed that SR reduced MMPs and boosted Col-II, aggrecan, and PG synthesis in rat chondrocytes with or without IL-1β (Yu et al., 2022). It also curbed IL-1β-induced β-catenin rise, diminishing inflammation. The multi-faceted influence of SR not only bolsters cartilage matrix integrity and maintains cellular viability but also holds substantial potential in hindering the progression of osteoarthritis. Through our investigative efforts focused on contiguous intervertebral discs, we discerned a conspicuous exacerbation in the magnitude of ASDD following spinal fusion, consequent to ovariectomy. This exacerbation coincided with a prominent upregulation in the manifestation of matrix metalloproteinases (MMPs), coupled with a concurrent downregulation in the expression of type II collagen, a pivotal constituent of the extracellular matrix. Moreover, the administration of SR demonstrated an obvious effect in decelerate the attrition of critical matrix components, while concurrently showing inhibitory effects on the generation of degradative enzymes.

Study limitations include the use of rats, which differ in walking patterns from humans, impacting the representation of age-related disc degeneration effects. Additionally, not using specific markers for cellular transformations may limit our understanding. The morphological nature of the Van Gieson stain is another constraint, as its focus on collagen and elastic fibers may not fully capture microvascular-related data.

In conclusion, our experiments demonstrate that SR can significantly slow down the progression of ASDD in osteoporotic conditions, with the underlying mechanism possibly being associated with preserving bone

mass to prevent spinal instability, maintaining the functional integrity of endplate vascular microstructure, and regulating matrix metabolism in the nucleus pulposus and annulus fibrosus. Osteoporosis often occurs around the same age as other degenerative diseases and can worsen their progression. Anti-osteoporosis medication SR treatments may not only maintain bone mass and prevent fractures, but early intervention could also potentially delay degenerative conditions linked to osteoporosis.

CRediT authorship contribution statement

Qi Sun: Writing – original draft, Resources, Project administration, Methodology, Investigation, Data curation. **Fang Liu:** Software, Resources, Project administration, Methodology, Investigation. **Jiakang Fang:** Resources, Project administration, Methodology, Investigation, Formal analysis, Data curation. **Qiangqiang Lian:** Project administration, Methodology, Investigation, Formal analysis. **Yupeng Hu:** Resources, Project administration, Methodology, Investigation, Formal analysis, Data curation. **Xinyu Nan:** Project administration, Methodology, Investigation. **Fa-Ming Tian:** Project administration, Methodology, Investigation. **Guochuan Zhang:** Writing – review & editing, Validation, Formal analysis, Data curation. **Dianwen Qi:** Validation, Supervision, Resources, Methodology, Investigation. **Liu Zhang:** Writing – review & editing, Validation, Conceptualization. **Jingwen Zhang:** Writing – review & editing, Validation, Supervision. **Yang Luo:** Validation, Supervision. **Zuzhuo Zhang:** Project administration, Methodology, Investigation. **Zhuang Zhou:** Writing – review & editing, Project administration, Methodology, Investigation, Funding acquisition, Conceptualization.

Declaration of competing interest

All authors disclosed no relevant relationships.

Data availability

Data will be made available on request.

Acknowledgements

This study was supported by a grant from National Natural Science Foundation of China, Youth Grant. Grant/Award Number: 81702180.

Appendix A. Supplementary data

Supplementary data to this article can be found online at https://doi.org/10.1016/j.bonr.2024.101744

References

Abe, Y., Takahata, M., Ito, M., Irie, K., Abumi, K., Minami, A., 2007. Enhancement of graft bone healing by intermittent administration of human parathyroid hormone (1-34) in a rat spinal arthrodesis model. Bone 41-5, 775–785.
(accessed 4 November /2013).
Allon, A.A., Aurouer, N., Yoo, B.B., Liebenberg, E.C., Buser, Z., Lotz, J.C., 2010. Structured coculture of stem cells and disc cells prevent disc degeneration in a rat model. Spine J. 10-12, 1089–1097.
Benneker, L.M., Heini, P.F., Alini, M., Anderson, S.E., Ito, K., 2004. Young investigator award winner: vertebral endplate marrow contact channel occlusions and intervertebral disc degeneration. Spine (Phila Pa 1976) 2005 (30–2), 167–173.
Bruyere, O., Delferriere, D., Roux, C., Wark, J.D., Spector, T., Devogelaer, J.P., Brixen, K., Adami, S., Fechtenbaum, J., Kolta, S., Reginster, J.Y., 2008. Effects of strontium ranelate on spinal osteoarthritis progression. Ann. Rheum. Dis. 67-3, 335–339.
Burch, M.B., Wiegers, N.W., Patil, S., Nourbakhsh, A., 2020. Incidence and risk factors of reoperation in patients with adjacent segment disease: a meta-analysis. J. Craniovertebr. Junction Spine 11-1, 9–16.
Calleja-Agius, J., Brincat, M.P., 2009. Effects of hormone replacement therapy on connective tissue: why is this important? Best Pract. Res. Clin. Obstet. Gynaecol. 23-1, 121–127.
Calvo, E., Castañeda, S., Largo, R., Fernández-Valle, M.E., Rodríguez-Salvanés, F., Herrero-Beaumont, G., 2007. Osteoporosis increases the severity of cartilage damage in an experimental model of osteoarthritis in rabbits. Osteoarthr. Cartil. 15-1, 69–77.
Chen, H., Zhou, X., Fujita, H., Onozuka, M., Kubo, K.Y., 2013. Age-related changes in trabecular and cortical bone microstructure. Int. J. Endocrinol. 2013, 213234.
Compston, J.E., McClung, M.R., Leslie, W.D., 2019. Osteoporosis. Lancet 393-10169, 364–376.
DePalma, A.F., Rothman, R.H., 1968. The nature of pseudarthrosis. Clin. Orthop. Relat. Res. 59, 113–118.
Dimar 2nd, J.R., Ante, W.A., Zhang, Y.P., Glassman, S.D., 1996. The effects of nonsteroidal anti-inflammatory drugs on posterior spinal fusions in the rat. Spine (Phila Pa 1976) 21–16, 1870–1876.
Dou, Y., Sun, X., Ma, X., Zhao, X., Yang, Q., 2021. Intervertebral disk degeneration: the microenvironment and tissue engineering strategies. Front. Bioeng. Biotechnol. 9, 592118.
Ebrahimkhani, M., Arjmand, N., Shirazi-Adl, A., 2021. Biomechanical effects of lumbar fusion surgery on adjacent segments using musculoskeletal models of the intact, degenerated and fused spine. Sci. Rep. 11-1, 17892.
Ensrud KE, Crandall CJ. Osteoporosis. Ann. Intern. Med. 2017;167-3:Itc17-itc32.
Etebar, S., Cahill, D.W., 1999. Risk factors for adjacent-segment failure following lumbar fixation with rigid instrumentation for degenerative instability. J. Neurosurg. 90-2 (Suppl), 163–169.
Fields, A.J., Ballatori, A., Liebenberg, E.C., Lotz, J.C., 2018. Contribution of the endplates to disc degeneration. Curr. Mol. Biol. Rep. 4-4, 151–160.
Gangji, V., Soyfoo, M.S., Heuschling, A., Afzali, V., Moreno-Reyes, R., Rasschaert, J., Gillet, C., Fils, J.F., Hauzeur, J.P., 2018. Non traumatic osteonecrosis of the femoral head is associated with low bone mass. Bone 107, 88–92.
Grangeat, A.M., Erario, M.L.A., 2023. The use of medical ozone in chronic intervertebral disc degeneration can be an etiological and conservative treatment. Int. J. Mol. Sci. 24–27.
Gruber, H.E., Gordon, B., Williams, C., Norton, H.J., Hanley Jr., E.N., 2007. Vertebral endplate and disc changes in the aging sand rat lumbar spine: cross-sectional analyses of a large male and female population. Spine (Phila Pa 1976) 32–23, 2529–2536.
Hart, D.J., Cronin, C., Daniels, M., Worthy, T., Doyle, D.V., Spector, T.D., 2002. The relationship of bone density and fracture to incident and progressive radiographic osteoarthritis of the knee: the Chingford study. Arthritis Rheum. 46-1, 92–99.
Henrotin, Y., Labasse, A., Zheng, S.X., Galais, P., Tsouderos, Y., Crielaard, J.M., Reginster, J.Y., 2001. Strontium ranelate increases cartilage matrix formation. J. Bone Miner. Res. 16-2, 299–308.
Ishihara, H., Osada, R., Kanamori, M., Kawaguchi, Y., Ohmori, K., Kimura, T., Matsui, H., Tsuji, H., 2001. Minimum 10-year follow-up study of anterior lumbar interbody fusion for isthmic spondylolisthesis. J. Spinal Disord. 14-2, 91–99.
Kamali, A., Ziadlou, R., Lang, G., Pfannkuche, J., Cui, S., Li, Z., Richards, R.G., Alini, M., Grad, S., 2021. Small molecule-based treatment approaches for intervertebral disc degeneration: current options and future directions. Theranostics 11-1, 27–47.
Kanis, J.A., Johansson, H., Oden, A., McCloskey, E.V., 2011. A meta-analysis of the effect of strontium ranelate on the risk of vertebral and non-vertebral fracture in postmenopausal osteoporosis and the interaction with FRAX(®). Osteoporos. Int. 22-8, 2347–2355.
Li, J., Xu, W., Zhang, X., Xi, Z., Xie, L., 2019. Biomechanical role of osteoporosis affects the incidence of adjacent segment disease after percutaneous transforaminal endoscopic discectomy, 14-1, p. 131.
Liu, C.C., Tian, F.M., Zhou, Z., Wang, P., Gou, Y., Zhang, H., Wang, W.Y., Shen, Y., Zhang, Y.Z., Zhang, L., 2015. Protective effect of calcitonin on lumbar fusion-induced adjacent-segment disc degeneration in ovariectomized rat. BMC Musculoskelet. Disord. 16, 342.
Liu, Q., Wang, X., Hua, Y., Kong, G., Wu, X., Huang, Z., Huang, Z., Liu, J., Yang, Z., Zhu, Q., 2019. Estrogen deficiency exacerbates intervertebral disc degeneration induced by spinal instability in rats. Spine (Phila Pa 1976) 44–9. E510-e9.
Liu, Q., Yang, Z., Liu, Y., Ji, W., Huang, Z., Liu, J., Lin, J., Hua, Y., Huang, Z., Wu, X., Zhu, Q., 2020. Cervical spinal instability causes vertebral microarchitecture change and vertebral endplate lesion in rats. J. Orthop. Translat. 24, 209–217.
Lou, C., Chen, H., Mei, L., Yu, W., Zhu, K., Liu, F., Chen, Z., Xiang, G., Chen, M., Weng, Q., He, D., 2017. Association between menopause and lumbar disc degeneration: an MRI study of 1,566 women and 1,382 men. Menopause 24-10, 1136–1144.
Luo, Y., Zhang, L., Wang, W.Y., Hu, Q.F., Song, H.P., Su, Y.L., Zhang, Y.Z., 2013. Alendronate retards the progression of lumbar intervertebral disc degeneration in ovariectomized rats. Bone 55-2, 439–448.
McKiernan, F.E., 2009. The broadening spectrum of osteoporotic vertebral fracture. Skeletal Radiol. 38-4, 303–308.
Mizrahi, J., Silva, M.J., Keaveny, T.M., Edwards, W.T., Hayes, W.C., 1993. Finite-element stress analysis of the normal and osteoporotic lumbar vertebral body. Spine (Phila Pa 1976) 18–14, 2088–2096.
Nachemson, A., Lewin, T., Maroudas, A., Freeman, M.A., 1970. In vitro diffusion of dye through the end-plates and the annulus fibrosus of human lumbar inter-vertebral discs. Acta Orthop. Scand. 41-6, 589–607.
O'Loughlin, P.F., Cunningham, M.E., Bukata, S.V., Tomin, E., Poynton, A.R., Doty, S.B., Sama, A.A., Lane, J.M., 2009. Parathyroid hormone (1-34) augments spinal fusion, fusion mass volume, and fusion mass quality in a rabbit spinal fusion model. Spine (Phila Pa 1976) 34–2, 121–130.
Pelletier, J.P., Kapoor, M., Fahmi, H., Lajeunesse, D., Blesius, A., Maillet, J., Martel-Pelletier, J., 2013. Strontium ranelate reduces the progression of experimental dog osteoarthritis by inhibiting the expression of key proteases in cartilage and of IL-1β in the synovium. Ann. Rheum. Dis. 72-2, 250–257.
Pelletier, J.P., Roubille, C., Raynauld, J.P., Abram, F., Dorais, M., Delorme, P., Martel-Pelletier, J., 2015. Disease-modifying effect of strontium ranelate in a subset of patients from the phase III knee osteoarthritis study SEKOIA using quantitative MRI:

reduction in bone marrow lesions protects against cartilage loss. Ann. Rheum. Dis. 74-2, 422–429.
Pradeep, K., Pal, B., 2023. Biomechanical and clinical studies on lumbar spine fusion surgery: a review, 61-3, pp. 617–634.
Reginster, J.Y., Sarlet, N., Lejeune, E., Leonori, L., 2005. Strontium ranelate: a new treatment for postmenopausal osteoporosis with a dual mode of action. Curr. Osteoporos. Rep. 3-1, 30–34.
Tat, S.K., Pelletier, J.P., Mineau, F., Caron, J., Martel-Pelletier, J., 2011. Strontium ranelate inhibits key factors affecting bone remodeling in human osteoarthritic subchondral bone osteoblasts. Bone 49-3, 559–567.
Tomé-Bermejo, F., Piñera, A.R., Alvarez, L., 2017. Osteoporosis and the Management of Spinal Degenerative Disease (II). Arch. Bone Jt. Surg. 5-6, 363–374.
Velnar, T., Gradisnik, L., 2023. Endplate role in the degenerative disc disease: a brief review. World J. Clin. Cases 11-1, 17–29.
Wáng, Y.X.J., 2018. Senile osteoporosis is associated with disc degeneration. Quant. Imaging Med. Surg. 8-6, 551–556.
Wang, T., Zhang, L., Huang, C., Cheng, A.G., Dang, G.T., 2004. Relationship between osteopenia and lumbar intervertebral disc degeneration in ovariectomized rats. Calcif. Tissue Int. 75-3, 205–213.
Xiao, Z.F., He, J.B., Su, G.Y., Chen, M.H., Hou, Y., Chen, S.D., Lin, D.K., 2018. Osteoporosis of the vertebra and osteochondral remodeling of the endplate causes intervertebral disc degeneration in ovariectomized mice. Arthritis Res. Ther. 20-1, 207.
Yu, H., Liu, Y., Yang, X., He, J., Zhong, Q., Guo, X., 2022. The anti-inflammation effect of strontium ranelate on rat chondrocytes with or without IL-1β in vitro. Exp. Ther. Med. 23-3, 208.
Yuan, C., Zhou, J., Wang, L., Deng, Z., 2022. Adjacent segment disease after minimally invasive transforaminal lumbar interbody fusion for degenerative lumbar diseases: incidence and risk factors. BMC Musculoskelet. Disord. 23-1, 982.
Zebaze, R., Atkinson, E.J., Peng, Y., Bui, M., Ghasem-Zadeh, A., Khosla, S., Seeman, E., 2019. Increased cortical porosity and reduced trabecular density are not necessarily synonymous with bone loss and microstructural deterioration. JBMR Plus 3-4, e10078.
Zhang, Y., Hannan, M.T., Chaisson, C.E., McAlindon, T.E., Evans, S.R., Aliabadi, P., Levy, D., Felson, D.T., 2000. Bone mineral density and risk of incident and progressive radiographic knee osteoarthritis in women: the Framingham study. J. Rheumatol. 27-4, 1032–1037.
Zhang, C., Shi, J., Chang, M., Yuan, X., Zhang, R., Huang, H., Tang, S., 2021. Does osteoporosis affect the adjacent segments following anterior lumbar interbody fusion? A finite element study. World Neurosurg. 146 e739-e46.
Zhou, Z., Tian, F.M., Wang, P., Gou, Y., Zhang, H., Song, H.P., Wang, W.Y., Zhang, L., 2015. Alendronate prevents intervertebral disc degeneration adjacent to a lumbar fusion in ovariectomized rats. Spine (Phila Pa 1976) 40–20. E1073–83.
Zhou, Z., Tian, F.M., Gou, Y., Wang, P., Zhang, H., Song, H.P., Shen, Y., Zhang, Y.Z., Zhang, L., 2016. Enhancement of lumbar fusion and alleviation of adjacent segment disc degeneration by intermittent PTH(1-34) in ovariectomized rats. J. Bone Miner. Res. 31-4, 828–838.